

PUBLISHED BY

# INTECH

open science | open minds

World's largest Science,  
Technology & Medicine  
Open Access book publisher



**2,850+**  
OPEN ACCESS BOOKS



**98,000+**  
INTERNATIONAL  
AUTHORS AND EDITORS



**91+ MILLION**  
DOWNLOADS



**BOOKS**  
DELIVERED TO  
151 COUNTRIES

AUTHORS AMONG  
**TOP 1%**  
MOST CITED SCIENTIST



**12.2%**  
AUTHORS AND EDITORS  
FROM TOP 500 UNIVERSITIES



Selection of our books indexed in the  
Book Citation Index in Web of Science™  
Core Collection (BKCI)

Chapter from the book *Nanocomposites and Polymers with Analytical Methods*  
Downloaded from: <http://www.intechopen.com/books/nanocomposites-and-polymers-with-analytical-methods>

Interested in publishing with InTechOpen?  
Contact us at [book.department@intechopen.com](mailto:book.department@intechopen.com)

# Silicon Based Composite Anode for Lithium Ion Battery

Angathevar Veluchamy<sup>1</sup> and Chil-Hoon Doh<sup>2</sup>

<sup>1</sup>Central Electrochemical Research Institute,

<sup>2</sup>Korea Electrotechnology Research Institute,

<sup>1</sup>India

<sup>2</sup>Republic of Korea

## 1. Introduction

The invention of Voltaic pile during 1800 by the Italian Physicist, Alessandro Volta brought new light and energy into the world through Direct Current (DC) producing device known as battery which performed operations in domestic, industrial and transport equipments. These batteries are divided broadly into two categories one the primary battery and the other rechargeable battery. Few examples of primary batteries are the non-aqueous lithium batteries, and the zinc and magnesium based batteries. The prominent and well established rechargeable batteries are lithium-ion, lead-acid, nickel-metal hydride and nickel-cadmium, silver-zinc systems (Balasubramanian et al., 1994, 1995; Jose Benedict et al., 1998; Renuka et al. 1992; Veluchamy et al., 2001, April 2009).

Recently, the cost escalation of petroleum fuel has turned the attention of policy makers and researchers toward battery powers systems in order to partly/completely replace the petroleum fuels for automotive applications. Among the battery systems considered for electric vehicle (EV) applications, the lithium ion batteries show promise of meeting both energy and power requirements. The possibility of developing high energy and safe lithium ion battery has been reinforced further by the statement of (Panasonic, 2010) which reports a silicon-carbon nanocomposite anode for the lithium ion battery, with 30% higher capacity than the graphite based lithium ion cells, has been intended to provide power to laptop computers during the fiscal 2012. To make economic viability and practical implementation, especially for EV application still more work has to be done on fronts such as improvements on energy/power capability and safety. To meet this requirement work has to be pursued on battery materials development with a special emphasis on cost and environments. For transport applications attempts have to be made to replace combustible organic electrolytes, oxygen releasing cathodes and reactive lithium anode. This chapter presents development of high specific capacity anode materials especially the silicon composite anode material for lithium ion batteries. The resource material for this chapter has been gathered from recent research publications on lithium anode materials development.

## 2. Anode development for lithium batteries

The early development on non-aqueous lithium battery began with lithium (Li) metal anode. Its use has been restricted to primary batteries and application to rechargeable systems was beset with dendrite growth over the Li anode. The dendrite appeared profusely

with cycling, in most cases punctured the separator, caused internal short between anode and cathode leading to rise of cell temperature which in the presence of organic electrolyte resulted in thermal runaway and in extreme cases cell explosion.

The discovery by (Yazami & Touzain, 1982, 1983) during 1980 that lithium could be inserted and de-inserted between the graphite layers and the report by (Mizushima et al., 1980) that lithium in 'lithium cobalt oxide' could be intercalated and de-intercalated made Sony Energytec in 1991 to roll the first lithium ion batteries into commercial market. Later, newer versions of lithium ion batteries with different cathodes such as lithium manganese oxide, lithium nickel oxide and lithium iron phosphate have been developed to meet different electrical requirement of the battery market. However, no break through was made on the development of anode materials to replace the graphite anode ( $\text{LiC}_6$ ).  $\text{LiC}_6$  has a theoretical capacity  $\sim 372 \text{ mAh g}^{-1}$ , which is only 10% of the lithium metal anode capacity ( $3800 \text{ mAh g}^{-1}$ ) and its practical capacity lied between 300 and  $350 \text{ mAh g}^{-1}$ . In addition to lower specific capacity it has other drawbacks such as first cycle irreversible capacity, capacity degradation with cycling and safety issues (Brummer et al., 1980; Huggins, 2002). In the mean time the announcement by Fujifilm that a new amorphous metal oxide has been introduced as negative electrodes for its lithium ion battery has turned the researchers still more vibrant especially to bring out newer high capacity anode materials for lithium ion batteries (Fujifilm, internet, 1996).

In the search for high capacity anode materials, silicon and tin apparently qualified as anode materials due to their high theoretical energy densities  $\sim 4190$  and  $\sim 990 \text{ mAh g}^{-1}$  corresponding to the formation of binary alloys  $\text{Li}_{22}\text{Si}_5$  and  $\text{Li}_{22}\text{Sn}_5$ . These anodes could not find immediate application because of their large volume variation  $\sim 328\%$  for 'Si' anode and  $\sim 258\%$  for 'Sn'. Among the two anode materials, much attention was paid on silicon anode. The reaction of lithium with elemental silicon was known for a long time. Prior to the findings that Li-Si alloy for Li-ion batteries it was exploited as a negative electrode for molten salt electrolyte batteries which operate at  $400^\circ\text{C}$  (Singh et al., 2004). The alloy forming reaction between 'Si' and 'Li' takes place when 4.4 atoms of Li combine with one atom of Si which is represented by the equation (1)



The volume increase of the product is 3.7 times that of the reactants. Such large crystallographic volume changes between the charged (alloyed) and discharged (de-alloyed) state cause stress in the electrode leading to internal cracks in the electrode. During cycling the electrode particles are pulverized into micro/nano particles. Such morphological changes results in loss of electrical contact, increased impedance leading to thermal run away and cell failure (Benedek & Thakeray, 2002).

### 3. Capacity degradation

The capacity degradation with cycling in a battery is attributed to volume variation of the electro-active masses. The magnitude of volume variations during lithium insertion and de-insertion differs for most anode/cathode materials which cause particle fracture. Every material has a characteristic terminal particle size beyond which the particle will not fracture or disintegrate. Particle with smaller sizes do not continue to fracture and it is recommended to employ smaller starting alloy particle in the electrode for better cycling behavior (Yang et al., 2007). Such finding encouraged research work on the synthesis and use of composites containing nano-particles.

The particle fracture causes electrical disconnection between the particles and current collector. The cause for such decrepitation/crumpling of electrode particles has been described through a simple one dimensional model which states that when two phase formation occurs simultaneously with volume mismatch the result will be the development of fracture in the material. If the two phases occurs with no change in the volume, the particle will not undergo fracture. Further the critical particle size could be bigger for a particle having greater toughness (Huggins & Nix, 2000).

It is also suggested micro-crack does not happen below a critical grain size. The predicted critical grain size is less than the unit cell size for a majority of single-phase materials. This suggests that it may not be practically possible to reach the particle size to solve the mechanical instability problem associated with Li-alloys (Wolfenstine, 1999). The following passage brings out published research work on silicon based anode which includes description of mechanism toward minimum volume changes of the electrode for better cycle characteristics.

#### 4. Silicon composite anode material - state of the art

In most of the research papers on silicon composite anode the insitu generated Cr-Si, NiSi<sub>2</sub>, NiSi, FeSi<sub>2</sub>, TiN, SiC, TiC, SiO<sub>2</sub> active nano- silicon, the externally added metal particles Fe and Cu, also the graphite and carbon blacks all serve to minimize the volume changes that arise during lithiation/de-lithiation of Si in the electrodes.

For both binary Li-Si and ternary Li-Si-Cr composites containing dendritic copper powder (Weydanz et al, 1999) obtained reversible capacities of about ~ 500 and 800 mAh g<sup>-1</sup> respectively. The higher capacity of 'Li-Si-Cr' composite is attributed to insitu generated Cr-Si phase which acts as an inactive conductive matrix along with active Li-Si phase.

Mg<sub>2</sub>Si/acetylene black composite reported by (Roberts et al, 2002) delivers an initial discharge capacity ~ 830 mAh g<sup>-1</sup> where the Li insertion into Mg<sub>2</sub>Si forms Li<sub>2</sub>MgSi which then tends to decompose into binary alloys, Li-Si and Li-Mg at low potential regions causing capacity degradation with cycling. (Cairns & Reimer, 2002) have also reported on magnesium silicide anode. (Chen et al., 2006) has reported on the preparation of nano structured Si/C composites.

(Shi et al, 2001) has shown the better reversibility of Li-Mg anode alloys prepared through Kinetically Controlled Vapor Deposition (KCVD) method is attributed to high diffusion coefficient of lithium atoms in the Li-Mg alloy compared to Li-Mg alloy prepared by reacting Mg and Li in molten states in a Glove box .

(Wolfenstine, 2003) reported two composite anodes, one made out of sieved CaSi<sub>2</sub> and the other ball milled CaSi<sub>2</sub> with carbon conductive material and found both materials showing not so promising results.

Through EDAX (Kim et al, 2000) reported a composite made of amorphous Si and nanosized TiN which gave a reversible capacity of 300 mAh g<sup>-1</sup> where TiN acted as a buffer matrix. In the nano-composite consisting of amorphous silicon and nano-crystalline TiC, the electrochemically inactive TiC served as a buffer matrix and the electrode delivered a reversible capacity of 380 mAh g<sup>-1</sup>(Guo, 2005).

(Park, 2005, 2006) obtained an alloy through arc-melting followed by high energy mechanical milling (HEMM) which consisted inactive phases NiSi<sub>2</sub>, NiSi and an active Si phases which delivered a reversible capacity of ~ 800 mAh g<sup>-1</sup>. (Wang et al 2000) showed that the NiSi/C nano-composite to perform better than Fe-Si nano-composite and found both electrodes exhibited capacity decline with cycling.

Composite with low Si content gave better cycle capacity  $\sim 600 \text{ mAh g}^{-1}$  even at 20<sup>th</sup> cycle where  $\text{FeSi}_2$  served as a volume buffer. The irreversible capacity usually observed between 0.9 and 0.7V is caused by electrolyte decomposition that contribute to passive film formation (Lee & Lee, 2002).

(Kim et al., 2005) achieved acceptable anode capacity for the multilayer films consisting of active (Si) and inactive (Fe) metal elements. (Dong, 2004) showed for a Fe-Si composite ( $\text{FeSi}_2 + \text{Si}$ )/C composed of a sandwich structure with the alloy particles in the middle core and the graphite layer at outer shells has exhibited high initial capacity  $\sim 680 \text{ mAh g}^{-1}$  with a reversible capacity  $\sim 500 \text{ mAh g}^{-1}$  even after 15 cycles. The good performance was attributed to the effective buffering of the volumetric changes of the Fe-Si particles by the graphite shell.

In (Zuo et al., 2006) the Si-Mn composites after 60 h ball milling showed best performance, especially when annealed at  $300 \text{ }^\circ\text{C}$  for 2 h, which had a reversible capacity of  $455 \text{ mAh g}^{-1}$ . Mn acted as an inactive buffer. The decline in cycle life was attributed to agglomeration of nano-sized Si-Mn particles. In another report the authors show that a Si-Mn-C composite annealed at  $200 \text{ }^\circ\text{C}$  exhibited an initial reversible capacity of  $463 \text{ mAh g}^{-1}$  retaining  $387 \text{ mAh g}^{-1}$  even after 40 cycles.

In (Wang et al., 2007) a composite prepared by incorporating silicon powder into an inverse emulsion polymerised resorcinol-formaldehyde (RF) followed by carbonization in an inert atmosphere gave  $910 \text{ mAh g}^{-1}$ . The addition of Cu further improved the cycling performance of the composite.

(Dimov et al., 2003) proposed trapping of lithium ions in the form of Li-Si alloy into the electrode takes place during cycling, making progressive decrease in the availability of lithium for extraction. Such decrease in capacity with cycling is responsible for the capacity fading with cycling in the carbon coated silicon powder. (Wilson et al., 1997) have pyrolysed 50 different silicon containing polymers including polysilanes, polysiloxane, pitch silane blends and showed through a diagram the extent of formation of SiC,  $\text{SiO}_2$  and C is due to pyrolyzation.

In (Lee et al., 2005) a carbon coated  $\text{Ni}_{20}\text{Si}_{80}$  alloy/graphite composite is presented with an improved cycle performance and reduced initial irreversible capacity loss attributed to buffering and conductive actions of the carbon coated graphite present in the composite. Around 200 compositions of combinatorial materials comprising Si-M (M = Cr + Ni, Fe, Mn) has been reported by (Fleischauer, 2005) where the anode capacity strongly depended upon Si content where the capacity varied from over  $3000 \text{ mAh g}^{-1}$  for nearly pure silicon to effectively zero for  $\sim 50\text{--}60\%$  of silicon.

Multiple component alloy composite (Dong et al., 2003) with Graphite/Ba-Fe-Si alloy has been observed to provide  $500 \text{ mAh g}^{-1}$  at 15<sup>th</sup> cycle.

Si-AB5 composite alloy (Zhang, 2007), where Fe is one of the components, exhibited initial and maximum reversible capacity  $\sim 370$  and  $385 \text{ mAh g}^{-1}$  with high capacity retention even after 50 cycles. The Si-AB5 composite containing 20 wt% Si provides discharge capacity  $\sim 420 \text{ mAh/g}$  with good capacity retention (72%) even after 50 cycles where the inactive AB5 alloy is said to accommodate large volume changes of Si nano-particles distributed on the surface of Si-AB5 composites during cycling.

(Zhang et al., 2004) reported, for the silicon-based thin film Si/TiN nano-composites formed by pulsed laser deposition method, better capacity attributed to dispersal of nanometer range amorphous Si particles in the presence of an inactive matrix of TiN.

Similarly the role of copper in  $\text{Cu}_5\text{Si-Si/C}$  anode has been explored and the report states that the anode delivered  $\sim 612 \text{ mAh g}^{-1}$  capacity with a capacity fade during initial cycles. The capacity fade formed was attributed to SEI film formation (NuLi, 2006).

(Kim, J. H. 2005) for a carbon coated Si-Cu<sub>3</sub>Si-Cu composite the copper silicide formed by pyrolysis is not an electro-active material and the improved performance of the composite was attributed to better electrical contact of metal silicide and pyrolyzed carbon.

A novel silicon/graphite material prepared by depositing a gelatinous silicon precursor over a porous natural graphite gave a stable 100 cycles at ~ 840 mAh g<sup>-1</sup> ascribed to good embedding of the silicon in the graphite matrix (Fuchsichler, 2011).

(Dimove et al., 2003) have deposited carbon over silicon through thermal vapour deposition using benzene or toluene as carbon source and nitrogen as a carrier gas. Among the three binary alloys of the type, Ti<sub>x</sub>Si<sub>y</sub> with variable x and y values only the carbon coated Ti-Si alloy exhibited good cycle performance, especially when the Si content in Ti-Si alloy is kept below the eutectic value of (Si + TiSi<sub>2</sub>) in the composite (Lee et al, December, 2006).

This part of the discussion has made clear that any one composite that is prepared with carbon coating, insitu generated inert phases with or without nano-active silicon particle produced during charge/discharge process deliver better electrochemical performances.

In the following sub headings the research contributions of the authors on the topic 'Silicon composite anode for lithium ion batteries' has been presented (Doh et al., Jan 2008, Feb 2008, April 2008, June 2008, May 2010; Veluchamy et al., Feb 2009, April 2009)

## 5. Experimental

### 5.1 Fe-Cu-Si/C composite anode

#### 5.1.1 Composite powder

Appropriate quantities of Cu (<10µm, 99% pure, Sigma-Aldrich), Fe (<53µm, 99.9% pure, High Purity Chemical Research Company, Japan) and Si (1-5µm, SI-100, >99 purity, AEE, NJ) with atomic ratio, Fe:Cu:Si = 1:1:2.5 were ball milled using a stainless steel (SS) grinding vial along with SS balls. The weight ratio of SS ball to the material was kept at 10:1 and the millings were carried out at 350 rpm. The vial was filled with argon gas and tightly closed with a gasket to prevent ingress of atmospheric oxygen. The material ball milled for 3h was then mixed with graphite in equal proportions in weight ratio, 50:50 and again ball milled for 24h. The composites ball milled for 3, 10, and 24h are hereinafter referred as 3HBM, 10HBM, and 24HBM, respectively. The composite thus arrived with the ratio Fe: Cu: Si = 1:1:2.5/graphite is represented as Fe-Cu-Si/C.

#### 5.1.2 Composite electrode

The composite powder from 5.1.1 was then blended with 10 wt% polyvinylidene difluoride (PVDF) dissolved in 1-methyl-2-pyrrolidinone in an agitator for 10 min to obtain a slurry mass. The slurry mass was coated onto a copper foil current collector and dried in a hot air oven at 110 °C for 2 h and pressed using a SS roller in order to reduce the thickness to ~ 75%. The active material coated copper foils were annealed at 110, 150, 200, and 250 °C in vacuum oven for 12 h.

#### 5.1.3 Cell construction

Annealed composite electrode was cut in the form of a circular disc of diameter 1.4 cm and coupled with lithium foil counter electrode separated by Celgard-2700 separator. The electrolyte from Techno Semichem. Ltd., Korea is 1M LiPF<sub>6</sub> dissolved in a co-solvent consisting of ethylene carbonate (EC) and ethyl methyl carbonate (EMC) in 1:1 (v/v) ratio with 2 wt% vinylene carbonate (VC). The coin cells assembled in a dry room maintained at ~21°C with dew point temperature between -65 and -70 °C were subjected to life cycle test

using charge-discharge analyzer, Toyo System, Ltd., Japan between 0 and 2V versus Li<sup>+</sup>/Li at a constant current of 0.253 mA cm<sup>-2</sup>.

### 5.1.4 XRD and SEM investigations

The ball milled composites were examined using Philips 1830 X-ray diffractometer with nickel-filtered Cu-K $\alpha$  radiation at a scan rate of 0.04° s<sup>-1</sup> over 2 $\theta$  range between 10–80°. The surface morphology of the active material coated copper foil was scanned using Hitachi S-4800 scanning electron microscope (SEM). In Fig. 1, the XRD pattern for Si, Cu, Fe, graphite powder(C), 3HBM-Fe-Cu-Si, 10HBM-Fe-Cu-Si, and 24HBM-{3HBM-Fe-Cu-Si:graphite = 50:50(w/w)} are presented.

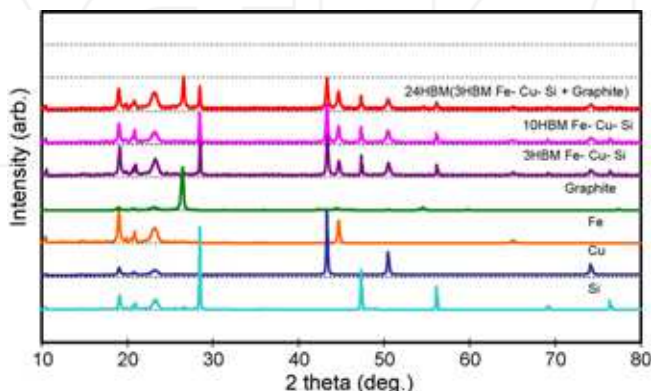


Fig. 1. XRD pattern of Fe, Cu, Si, C, 3HBM- Fe-Cu-Si, 10HBM- Fe-Cu-Si, and 24HBM-{3HBM- Fe-Cu-Si: C = 50:50(w/w)}.

All these suggest ball mill duration does not change the elemental particles, rather reduces them into smaller particulates as evident from the minimum change in the intensity of Bragg's peak in the XRD patterns.

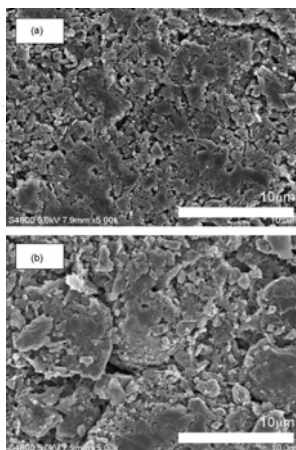


Fig. 2. SEM pictures of Fe-Cu-Si /C composite electrode annealed. Electrode --'a' at 110 °C and electrode ---'b' at 200 °C.

The SEM pictures of Fe-Cu-Si/C composite with PVDF binder annealed at 110 °C was compared with the best performing electrode annealed at 200 °C and presented in Fig. 2 as 'a' and 'b', respectively. The pictures show the cathode particles in 'b' remain in agglomerated state with boundaries and distinct interspaces compared to that of the particles in 'a' with particle sizes varying from  $< \sim 1$  to  $\sim 10$   $\mu\text{m}$ . Such interfaces and voids formed in the composite electrode annealed at high temperature is expected to provide better ionic pathway for the ions thereby providing better conductivity and also the voids are expected to minimise the volume change of the electrode during charge/discharge cycles.

The superimposition of Bragg's peaks appearing in the XRD pattern of individual materials such as Si, Cu, Fe over the XRD spectrum of Si, Cu, Fe & graphite composite shows that the superimposed XRD spectrum coincide exactly with spectrums obtained for 3HBM- Fe-Cu-Si, 10HBM- Fe-Cu-Si, and 24HBM-{3HBM-Fe-Cu-Si: C (graphite) = 50:50(w/w)} respectively.

### 5.1.5 Charge/discharge characteristics

The typical discharge-charge profiles for the electrode Fe-Cu-Si/C annealed at 200 °C presented in Fig. 3 shows the initial lithiation and delithiation capacities respectively are 809 and 464 mAh  $\text{g}^{-1}$ . The capacity difference between the two processes is 345 mAh, nearly 42% of the initial lithiation capacity. This implies that during the first cycle  $\sim 42\%$  of Li is retained within the electrode as irreversible capacity. This irreversible capacity is due to the reaction of graphite, metal particles and silicon with the chemically bonded or adsorbed oxides present within the electrode. During the initial discharge, inserted lithium reacts irreversibly at first with these oxides and water impurities forming  $\text{Li}_2\text{O}$ , and then forms  $\text{Li-Si}$  and  $\text{LiC}_6$ . The amount of  $\text{Li}_2\text{O}$  formed is proportional to irreversible capacity during cycling. Thus formed  $\text{Li}_2\text{O}$  along with Fe, Cu and Graphite acts as a buffer, absorbs the volume expansion/contraction during discharge/charge process. Also other products formed due to oxidation of electrolyte and binder along with  $\text{Li}_2\text{O}$  are  $\text{Li}_2\text{CO}_3$ , LiF and alkyl carbonates. All these products forms part of SEI films of silicon and graphite.

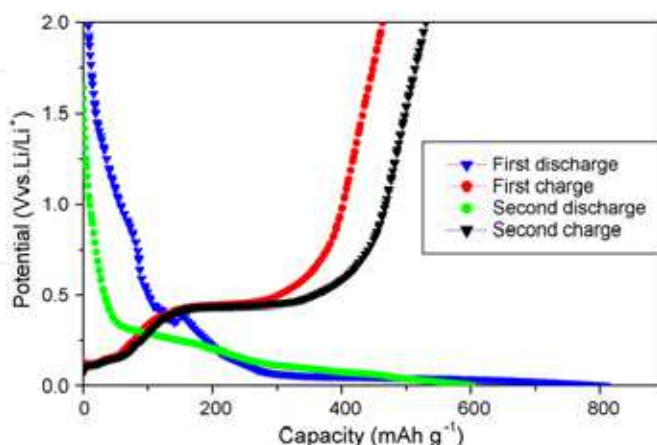
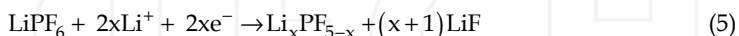
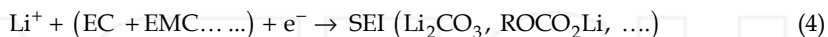
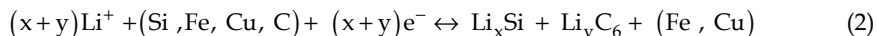


Fig. 3. Discharge-charge profiles for Fe-Cu-Si/C composite electrode annealed at 200 °C.

For the present system we propose the following reactions that are responsible for the reversible reaction (2) and irreversible reactions such as lithium oxide formation reaction (3), organic solvent decomposition reaction (4), & electrolyte decomposition reaction (5).



In addition to the reactions (3), (4) and (5) other contributing factors responsible for capacity degradation with cycle life are particle fracture followed by loss of electrical contact between the electro-active species and also between electro-active species & current collector (Aurbach & Schechter, 2004). In the second cycle the discharge and charge capacities respectively are 607 and 531 mAh g<sup>-1</sup> which shows a considerable reduction in irreversible capacity equal to ~12%. The authors in (NuLi, 2006; Wang, 2007; & Aurbach, 2004&2005) describe that the irreversible capacity in the graphite electrode is due to the reaction of intercalated Li with the adsorbed oxygen and solvent molecules leading to the formation of SEI film over the graphite particles which comprises mainly LiF, Li<sub>2</sub>CO<sub>3</sub> and ROCO<sub>2</sub>Li etc.

#### 5.1.6 Capacity with cycle number at different electrode annealing temperatures

The discharge and charge capacities of the electrodes annealed at different temperatures are depicted in Fig. 4 and Fig. 5 respectively.

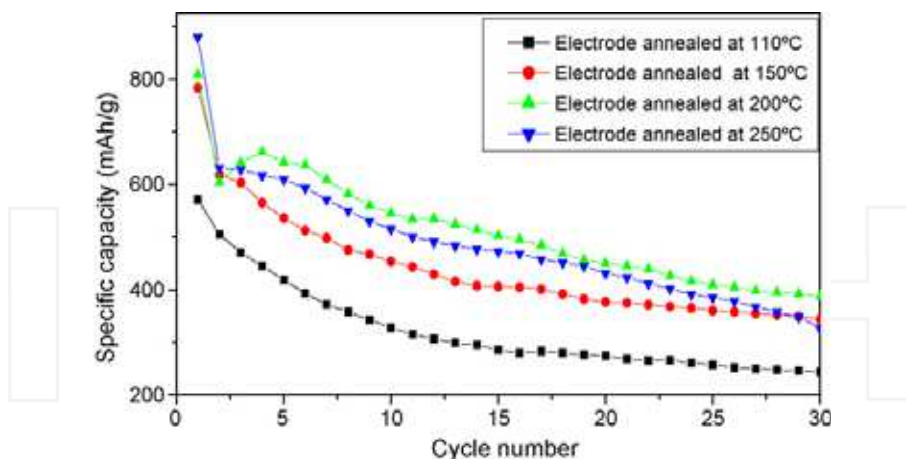


Fig. 4. Discharge capacity as a function of cycling with electrode annealing temperature.

The Fig. 4 shows an improvement of discharge capacity with annealing temperature. The curve shows discharge capacity 387 and 327 mAh g<sup>-1</sup> for the electrode annealed at 200 and 110°C respectively at 30<sup>th</sup> cycle. In Fig. 5 the initial charge capacity values for charging process remains at a low value, after few cycles the capacity raises and then stabilizes in the

subsequent cycles. The gain in charge/discharge capacity after the first cycle in all four temperature except at 110°C (Fig.4 & 5) is attributed to realignment/redistribution of constituents of the SEI film. The higher capacity obtained for the electrode annealed at 200 °C could be attributed to enhanced electrical conductivity and easy ionic diffusion of the electrode.

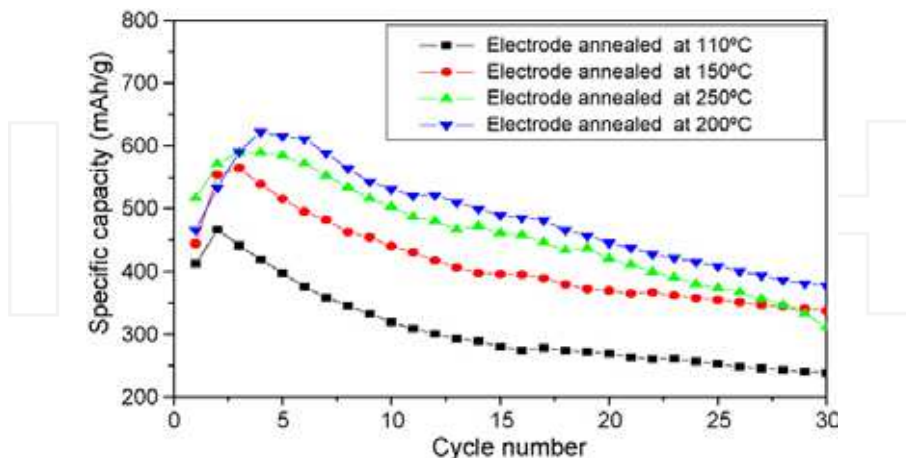


Fig. 5. Charge capacity as a function of cycling with electrode annealing temperature

Further support for the improved capacity of the annealed electrodes could be understood from the SEM picture which shows well separated electrode particulates with interspaces between the electrode particles which is expected to favour ionic diffusivity and electrochemical behaviour. Similar reports have been presented by (Zuo et al., 2006) for SiMn/C anode which exhibited improved reversible capacity (426 mAh g<sup>-1</sup>) for the electrode annealed at 200 °C.

### 5.1.7 Irreversible capacity loss

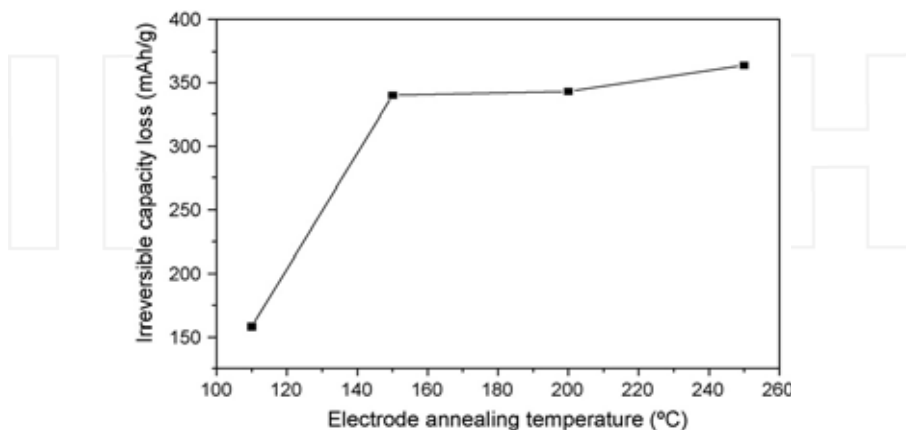


Fig. 6. Irreversible capacity loss as a function of electrode annealing temperature.

The Fig.6 illustrates irreversible capacity loss by Fe-Cu-Si/C electrode during first cycle (lithiation process) for the electrodes annealed at different temperatures. The curve shows higher irreversible capacity for the electrodes annealed above 150 °C. The high temperature annealing causes better particle segregation which makes easy diffusion of lithium ions and effective conversion of all adsorbed oxides present in the electrode into  $\text{Li}_2\text{O}$  (reaction 3). The high charge consumption for SEI film formation in Cu-Si alloy (NuLi, 2006) anode has been explained as due to increase of surface area through longer ball milling duration.

## 5.2 SiO/C composite anode

### 5.2.1 Composite preparation

Equal proportions of SiO (Aldrich, -325 mesh) and graphite (Sodiff New Materials Co. Ltd., Korea, -400 mesh) powders were placed together in a 200 ml stainless steel (SS) vial. The weight ratio of the SS ball to the material was maintained at 10:1 and the vial was filled with argon gas. The contents in the vial were milled for 12, 18, 24 and 30 h by means of high-energy ball milling (HEBM) at 350 rpm and four different samples were collected. The samples were subjected to physical and electrochemical investigation following the procedures as in 5.1.4 and 5.1.5.

### 5.2.2 XRD and SEM Investigation

The XRD patterns for the starting materials SiO, graphite(C) and milled SiO/C composites are presented in Fig. 7. The XRD pattern shows that the graphite considered for ball milling is crystalline whereas SiO is amorphous. The patterns for milled SiO/C samples reveal that the peak corresponding to graphite decreases with increase in ball mill duration and also no new peaks observed. This suggests that ball milling causes only particle size reduction of the graphite and does not produce any new compound.

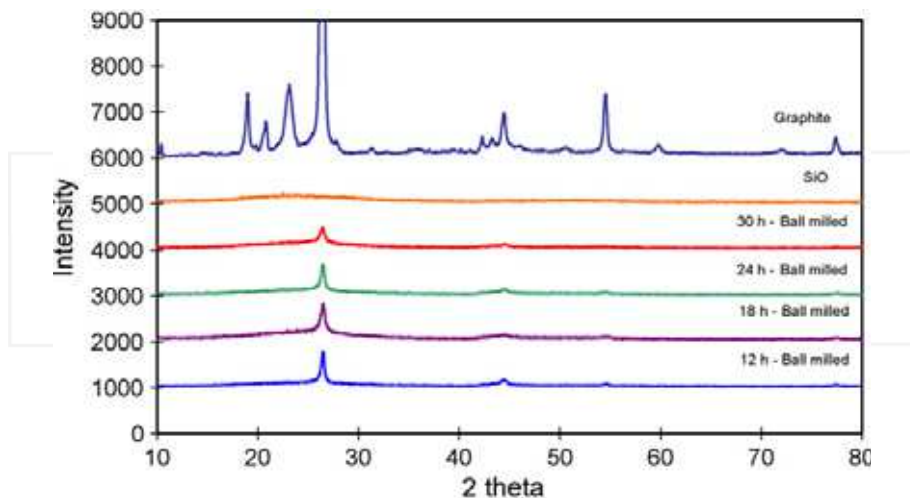


Fig. 7. XRD patterns of SiO, graphite (C), and samples (SiO and graphite) ball-milled for different durations.

The scanning electron micrographs (SEM) of samples ball-milled for different durations are given in Fig. 8. The SEM pictures show a gradual decrease in the crystallinity of the particulates of the samples with ball mill duration which is in accordance with the XRD patterns. The particles in the sample milled for 12 h exist as discrete crystalline particles whereas the 30 h-milled sample lacks definite particle shape and shows continuity in the particle distribution. In some domains, the particle distribution in the 24 h ball-milled sample remains between 5 and 20  $\mu\text{m}$  whereas in other regions the continuity is maintained.

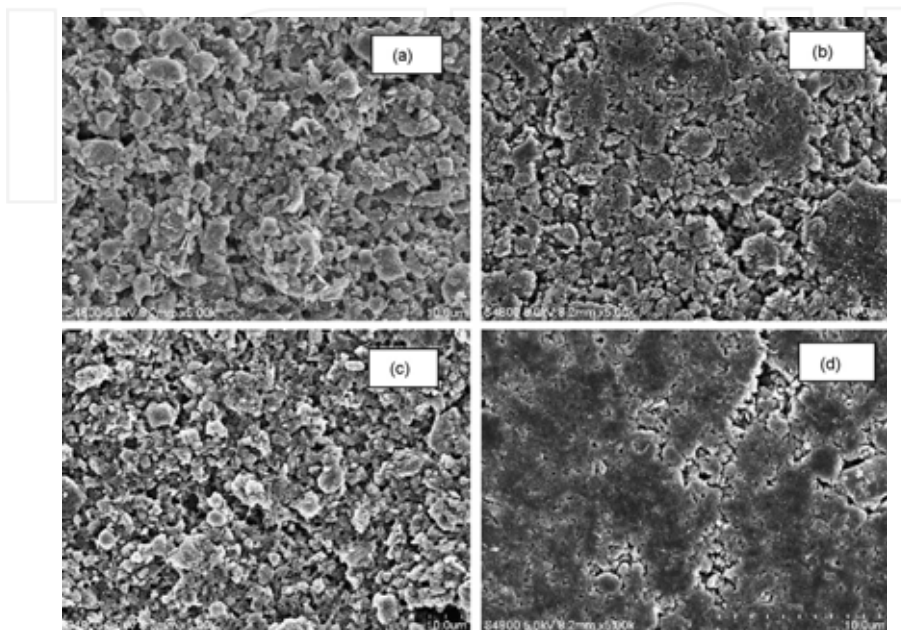


Fig. 8. SEM micrographs of samples (SiO and graphite) ball-milled for different durations: (a) 12 h; (b) 18 h; (c) 24 h; (d) 30 h.

### 5.2.3 Charge/discharge characteristics

The composite powder from the section 5.2. 1 has been coated over copper foil following the procedures described in 5.1.2 and cell was fabricated as described in 5.1.3 to get SiO/C anode for electrochemical characterization study. A typical discharge-charge profile of the SiO/C composite electrode is given in Fig. 9. The difference between the initial discharge ( $1556 \text{ mAh g}^{-1}$ ) and charge ( $693 \text{ mAh g}^{-1}$ ) capacities equal to 55% of capacity is known as irreversible capacity. In the second cycle, the irreversible capacity is reduced to 14%. It is well known that during the first lithiation process, lithium reacts with SiO and forms nano-silicon and  $\text{Li}_2\text{O}$ . The nano-silicon then reacts with Li and forms Li-Si alloy (Lee & Lee, 2004). Contrary to this explanation (Miyachi et al., 2006) showed through O 1s spectra analysis that during the first lithiation process a direct absorption of Li by SiO takes place giving rise to the formation of  $\text{Li}_4\text{SiO}_4$  and  $\text{Li}_2\text{O}$ .

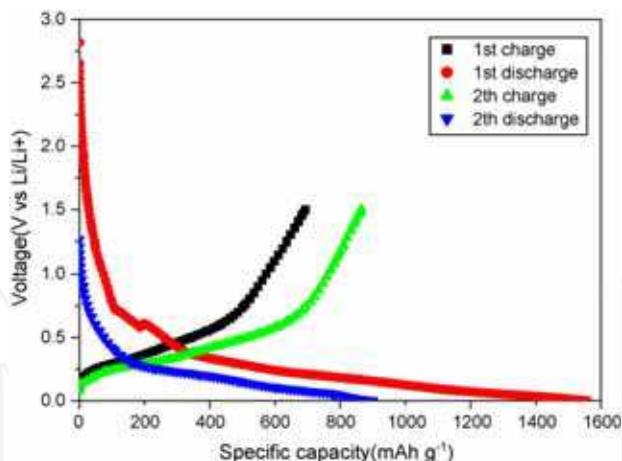


Fig. 9. Voltage - specific capacity profile of the SiO/C composite electrode

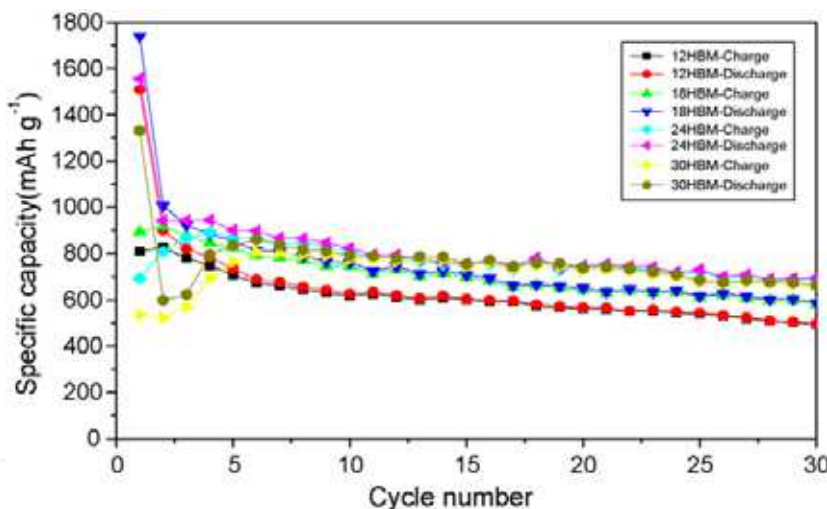


Fig. 10. Specific capacity - cycle number for the electrodes with ball mill durations

Among the composites prepared, the 24 h ball-milled sample exhibits higher reversible capacity. This might be attributed to optimum particle size distribution at 24 h ball milling which provided better lithium ion diffusion compared with other compositions. The loss of capacity shown by the sample with cycling could be attributed to trapping of  $\text{Li}^+$  ions within the electrode particles and decomposition of the organic solvent toward formation of SEI film. The other factors responsible for capacity degradation with cycling are particle fracture and loss of electrical contact between electro-active species and current-collector.

The discharge and charge capacity values for the initial and 30th cycles obtained from Fig. 10 are listed in Table 1. The total irreversible capacity is due to irreversible reaction between Li reacting with, 1) SiO into forming  $\text{Li}_2\text{O}$  through the reaction  $\text{SiO} + 2\text{Li}^+ \rightarrow \text{Si} + \text{Li}_2\text{O}$ , 2) oxygen impurities present in the graphite, and 3) electrolyte and binders during initial charging. These

reaction products form the SEI film which constitute organic and inorganic carbonates, Fluorides, oxides etc., (Datta & Kumta, 2007; Aurbach, 2002 & 2005).

<i>Ball mill duration</i> (h)	1st cycle			30 <sup>th</sup> cycle	
	<i>Discharge capacity</i> (mAh/g)	<i>Charge capacity</i> (mAh/g)	<i>Irreversible capacity</i> (%)	<i>Discharge capacity</i> (mAh/g)	<i>Charge capacity</i> (mAh/g)
12	1508	809	46	495	493
18	1738	892	48	589	580
24	1556	693	55	696	688
30	1330	535	59	663	656

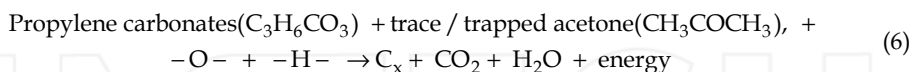
Table 1. The capacity values arrived at 1<sup>st</sup> and 30<sup>th</sup> cycle at different ball mill duration.

The reversible and irreversible capacity values appear to be interdependent as their values show simultaneous increase until the 24h ball-milled sample. This interdependency also explains the beneficial role played by a higher percentage of Li<sub>2</sub>O which buffers the volume change during the alloying and de-alloying processes.

### 5.3 Carbon coated SiO/C composite anode

#### 5.3.1 Composite preparation

This part compares performance of two composites. One composite prepared by ball milling equal proportion of 'SiO' and 'C' for 15 h, named as SiO/C composite and denoted as 'A' by following the same procedure described 5.2.1. Another composite is prepared by mixing 2.5 g of the composite 'A' in 5 ml of the solution made of propylene carbonate (PC) and acetone (AC) in the ratio 1:1 (v/v) in a beaker using a magnetic stirrer. During stirring the volume of the slurry will be reduced due to the evaporation of acetone. The slurry was poured into an alumina boat and heated in a furnace at a rate of 5 °C under an argon atmosphere and maintained at 750 °C for 3 h and then spontaneously cooled down to reach room temperature. Thus obtained composite is named as composite 'B'. The thermal decomposition of the organic molecules (Ng et al., 2007) under argon atmosphere in the presence of SiO/C composite may be represented by the equation (6)



The components -O- and -H- come from trace of adsorbed water molecules and also from physically/chemically attached -O- from SiO and graphite. In C<sub>x</sub>, the x value of carbon varies from 1 to 3. The material obtained after thermal treatment of the slurry appeared as agglomerated clusters presumably due to wrapping up of C<sub>x</sub> carbon particles which upon crushing in a mortar converted into a powder named as composite 'B'. Similar approach has been followed by (Ng et al,2007) for carbon coating of silicon.

#### 5.3.2 XRD and SEM investigation

The XRD pattern obtained for SiO, graphite (C) and the composite 'A', and the composite 'B' are presented in Fig. 11. The pattern for composite 'A' shows that the graphite considered for ball milling is crystalline one and SiO is an amorphous variety. Thermally treated organic slurry composite powder shows a slight enhancement of the amplitude of the peak at 26° showing enhanced crystalline nature of the graphite. Further this XRD pattern

suggests ball milling and the heat treatment with organic solutions have not produced the formation of any new compound.

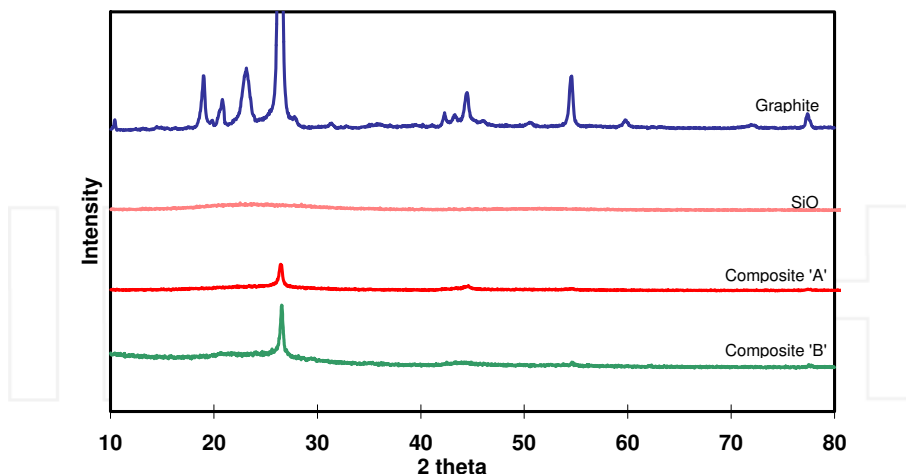


Fig. 11. XRD pattern of SiO; Graphite(C); Ball milled SiO/C Composite  $\rightarrow$  'A'; Blend made of (SiO/C + PC + AC) and heated to 750 °C for 3 h  $\rightarrow$  'B'.

The SEM pictures of the electrode-A and electrode-B are shown in Fig. 12. It is evident from the SEM pictures that the electrode-B has larger particles with voids and interspaces compared to the particle arrangement in the electrode-A. The partial removal of oxygen and trace -H- present in the composite could have effected bonding rearrangement within the particles invoking reinforcement and compactness to the resultant structure in concomitant with trapping/wrapping by formed C<sub>x</sub> particles.

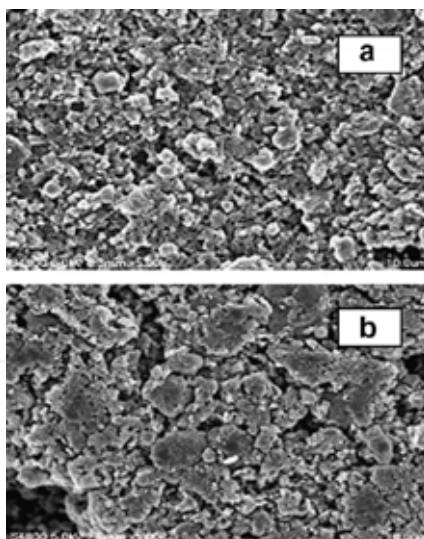


Fig. 12. SEM micrographs of samples, a- Electrode -A; b- Electrode- B

The comparative curves showing the values of specific capacity with cycle number for the electrode-A and electrode-B are given in Fig. 13. The figure illustrates that the electrode-A exhibits higher charge/discharge capacity values until 53rd cycle and then the capacity falls below the value of the electrode-B. The initial irreversible capacities (863 mAh g<sup>-1</sup> for the electrode-A and 733 mAh g<sup>-1</sup> for electrode-B) denote the utilization of these capacities for the formation of SEI film Li<sub>2</sub>O. SEI film protects the anode and Li<sub>2</sub>O acts as a buffer component for improving the cycle behavior. The difference in irreversible capacities (863-733= 130 mAh g<sup>-1</sup>) suggests lowering of 130 mAh g<sup>-1</sup> capacity in the composite -B compared to the electrode-A. From this we can infer that 130 mAh g<sup>-1</sup> equivalent of oxygen/water molecule are chemically/physically present in the composite 'A' which is absent in the composite 'B'. During carbon coating these oxygen/water molecules could have liberated as CO<sub>2</sub>. This also suggests that Li<sub>2</sub>O in composite-B is lower by 130 mAh g<sup>-1</sup> capacity equivalent compared to that in composite-A. Even though the electrode-B has lower buffer component than in electrode-A, it shows better cycle behavior, attributed possibly to structural rearrangement during partial removal of oxygen/water and wrapping of the electrode particle by C<sub>x</sub> to form a well reinforced but a flexible structure to allow Li<sup>+</sup> ion diffusion for making the electrode-B to withstand the volume changes during cycling. It may be noted from 1st to 4th cycle for the electrode-A, the charge capacity value increases from 693 to 890 mAh g<sup>-1</sup> and for the electrode-B from 613 to 652 mAh g<sup>-1</sup>. The increase in the charge capacity values calculated as 197 and 39 mAh g<sup>-1</sup> may be termed as the charge capacity recovery values for the respective electrode-A and electrode-B. The attributes of the electrode-B such as lower charge capacity recovery and lower capacity degradation with cycling further support the favourable structural rearrangement that occurred during thermal treatment with organic solution.

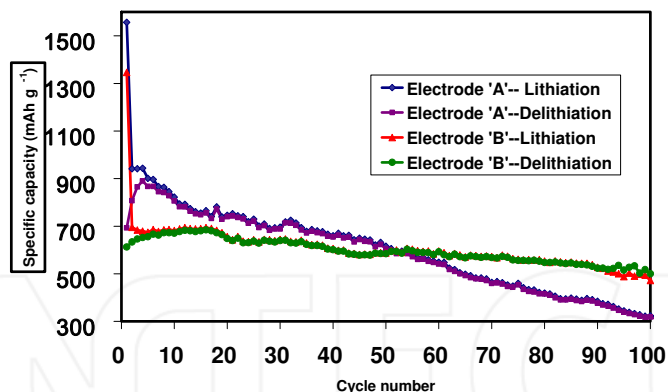


Fig. 13. Specific capacity as a function of cycle number for Electrode-A and Electrode-B

The cyclic voltammograms of the electrode-A and electrode-B scanned between 0 and 1.5 V at a scan rate of 0.1 mV s<sup>-1</sup> is shown in Fig. 14. The delithiation process displayed in the 5th cycle is considered for discussion. The delithiation process of the electrode-A is associated with an increase of current with potential whereas the electrode-B shows an increase of voltage by 0.3 V but exhibits nearly a stable current between 0.3 and 0.6 V. This shows the over-potential dependent current flow through the electrode-A which is possible for an electrode with a loosely bound dispersed structure. The electrode-B nearly does not show increase of current as the potential is scanned from 0.3 to 0.6 V, illustrating that the

electrode-B behaves apparently like a resistor over this narrow potential range. The resistor like behaviour illustrates the compact nature of the structure which could streamline the current flow with a tolerable volume change during charge/discharge process. This is well supported by the SEM micrographs which show the presence of large interspaces and voids among the agglomerated particles. These voids and interspaces could accommodate enough electrolytes for easy lithium ion diffusion. Since the capacity degradation is less with cycles it may be presumed that the electrode has a flexible structure with sufficient pores to buffer the volume changes during charge/discharge cycles.

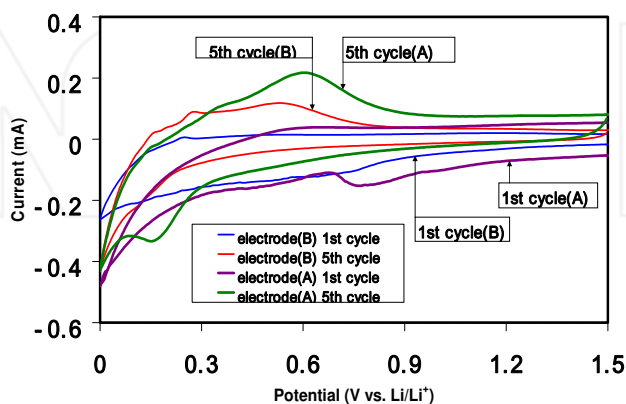


Fig. 14. Cyclic voltammogram for Electrode-A and Electrode-B at  $0.1\text{mVs}^{-1}$ .

## 5.4 Thermochemically generated $\text{Li}_4\text{SiO}_4$ phase in the composite

### 5.4.1 Composite preparation

Equimolecular quantities of lithium hydroxide monohydrate  $\text{LiOH} \cdot \text{H}_2\text{O}$  (Aldrich) and  $\text{SiO}$  ( $-325$  mesh, LTS Chemicals Inc.) were mixed in a mortar and then heated to  $550^\circ\text{C}$  for 3 h in an argon atmosphere. Graphite (C) was then added to maintain the weight ratio of C and  $\text{SiO}$  at 1:1 and ball-milled for 15 h. The composite was named as 'A'. In order to understand the behaviour of the new composite 'A' another composite 'B' was prepared by just ball milling  $\text{SiO}$  and C in a weight ratio of 1:1 for 15 h. The samples were subjected to physical and electrochemical investigation following the procedures described in sections 5.1.4 and 5.1.5 in the following section.

### 5.4.2 X-ray diffraction analysis

The XRD patterns of graphite (C),  $\text{SiO}$ ,  $\text{LiOH}$ , heat-treated ( $\text{SiO} + \text{LiOH}$ ) and ball-milled material made of heat-treated ( $\text{SiO} + \text{LiOH}$ )/C presented in Fig. 15 shows graphite(C) and  $\text{LiOH}$  are crystallites, and  $\text{SiO}$  is amorphous. The constituents C,  $\text{SiO}$  and  $\text{LiOH}$  are noted in figure as (a) (b) and (c). The precursor material obtained by heating ( $\text{SiO} + \text{LiOH}$ ) at  $550^\circ\text{C}$  does not show peaks corresponding to  $\text{LiOH}$  but exhibits new peaks. Examination with the JCPDS file shows that the new peaks are related to the compound  $\text{Li}_4\text{SiO}_4$ . Also the base line above the horizontal line between  $2\theta$  values  $20^\circ$  and  $30^\circ$  suggests the presence of  $\text{SiO}$  in the heat-treated materials. In the sub-section XR-2, the material (d) = (b) + (c) heated to  $550^\circ\text{C}$  exhibits a peak at  $2\theta = 32^\circ$  which could be ascribed to  $\text{Li}_4\text{SiO}_4$  and not to  $\text{Li}_2\text{O}$  as there exists no other peak that can be attributed to  $\text{Li}_2\text{O}$ .

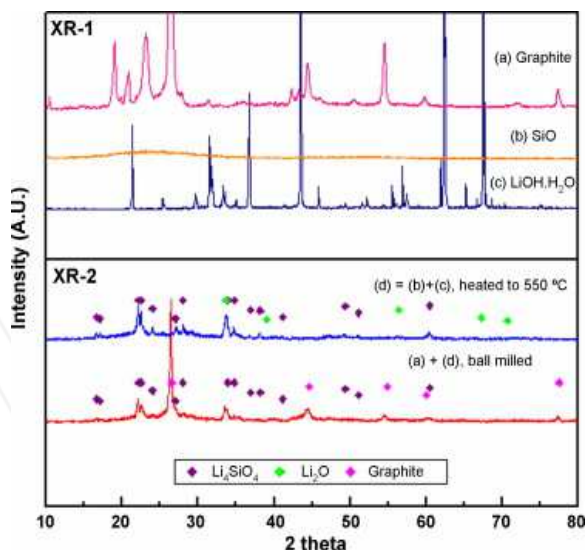


Fig. 15. XRD pattern of materials: (a) graphite; (b) SiO; (c) LiOH; (d) = (b) + (c) heated at 550 °C in argon atmosphere; (a) + (d) ball-milled composite material.

This observation leads to the conclusion that all the  $\text{Li}_2\text{O}$  has reacted with SiO at 550 °C to form  $\text{Li}_4\text{SiO}_4$ . There are also several minor peaks for  $\text{Li}_4\text{SiO}_4$ . Hence, it may be proposed that before the melting point (from ~450 to 470 °C) the lithium hydroxide is dehydrated to form  $\text{Li}_2\text{O}$  as represented by reaction (7). The reaction of  $\text{Li}_2\text{O}$  with SiO may be represented by reaction (8)



Reaction (8) indicates the product contains nano-silicon,  $\text{Li}_4\text{SiO}_4$  in addition to SiO in the precursor material (d). The compound  $\text{Li}_4\text{SiO}_4$  has a high negative free energy change ( $\Delta G^\circ_{298\text{K}} = -2366 \text{ kJ/mole}$ ) (International, 2004) and is considered to be an electrochemically inactive species in the composite (yang, 2007). The XRD pattern of the ball milled materials (d) with graphite (a) shows a reduction in the peak heights of both graphite and  $\text{Li}_4\text{SiO}_4$  which implies these particles have undergone size reduction during ball milling.

### 5.4.3 Cycle/capacity behaviour

The variation of specific capacity with cycle number for electrodes 'A' and 'B' is presented in Fig. 16. Data obtained from Fig. 16 is presented in Table 2. The irreversible capacity 387  $\text{mAh g}^{-1}$  (44%) exhibited by electrode 'A' is considerably lower compared to ~863  $\text{mAh g}^{-1}$  (55%) as shown by electrode 'B'.

The electrode 'A' also exhibits a lower initial lithiation capacity (862  $\text{mAh g}^{-1}$ ) than electrode 'B'. The reduction in initial capacity and also the irreversible capacity are attributed to the reduction of  $\frac{1}{4}$  part of SiO in the composite 'A', which has been converted into  $\text{Li}_4\text{SiO}_4$  during precursor formation. The amount of SiO present in the composite has a direct relationship with irreversible capacity and initial specific capacity, which is in agreement with an early report (Doh et al., May 2008). The slightly higher charge capacity shown by electrode 'A', even

at the 100th cycle could be attributed to the buffer action provided by  $\text{Li}_4\text{SiO}_4$ . The capacity values such as initial lithiation, initial delithiation, irreversible capacity and charge capacity values obtained for the electrode 'A' and electrode 'B' is presented in the Table. 2 which illustrate the superior quality of thermochemically treated composite over the untreated.

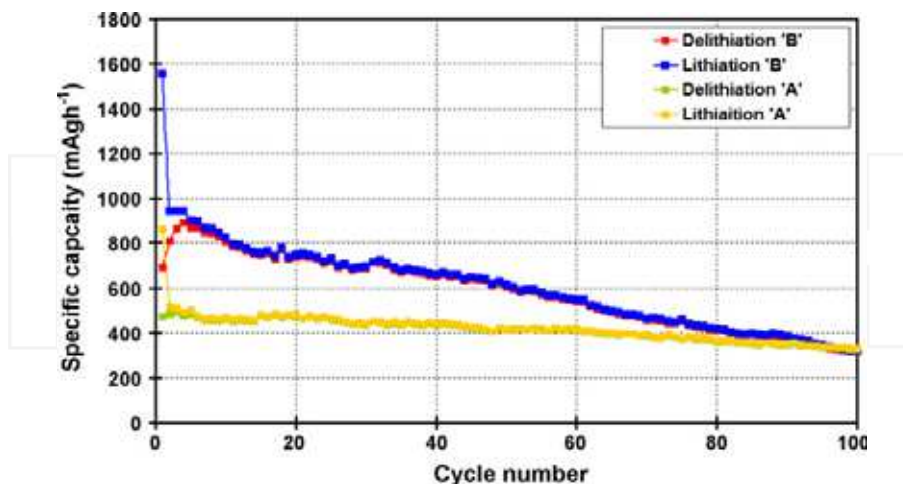


Fig. 16. Profile of specific capacity versus cycle number: delithiation 'B' and lithiation 'B' represent charge and discharge curves, respectively, for SiO/C electrode 'B'; delithiation 'A' and lithiation 'A' represent charge and discharge curves for heat treated (SiO + LiOH)/C electrode 'A'.

Composition of the electrodes	Initial lithiation capacity (mAh g <sup>-1</sup> )	Initial delithiation capacity (mAh g <sup>-1</sup> )	Irreversible capacity (mAh g <sup>-1</sup> )	Charge capacity at 100th cycle (mAh g <sup>-1</sup> )
Heat-treated (SiO + LiOH) with C electrode 'A'	862	475	387 (44%)	333
SiO with C electrode 'B'	556	693	863 (55%)	318

Table. 2 Capacity values obtained from Fig. 16 for two different composite electrodes.

## 5.5 Comparative performance

### 5.5.1 Composites with SiO, Si and graphite as constituents

The Charge/discharge and cycle capability for four different composites each containing 4g of C (Graphite or graphite with carbon) along with constituents Si and SiO are compared in the Fig. 17 and the data from the figure is presented in the Table 3.

The table shows maximum delithiation capacity values for the composite (a) is 1400 mAh g<sup>-1</sup> at 4<sup>th</sup> cycle for Si:SiO:C = 3:1:4, for (b) is 1450 mAh g<sup>-1</sup> at 8<sup>th</sup> cycle for Si:SiO:C = 2:2:4, for (c) is 870 mAh g<sup>-1</sup> at 4<sup>th</sup> cycle for SiO:C = 1:1, and for (d) the carbon coated composite SiO:C = 1:1 is 700 mAh g<sup>-1</sup> at 16<sup>th</sup> cycle. The same composites show delithiation capacities at 50<sup>th</sup> cycle for the composite (a) 480, for (b) 750, for (c) 610, and for (d) 580 mAh g<sup>-1</sup>. Therefore, the capacity retentions at the fiftieth cycle compared to maximum specific capacity values are

34%, 52%, 70%, and 83% for electrodes (a), (b), (c), and (d), respectively. Fig. 17 and Table-3 show electrode with lower silicon content exhibit better electrochemical performance.

Electroactive material in the electrode (ratio)	1 <sup>st</sup> LC	1 <sup>st</sup> DLC	1 <sup>st</sup> IRC	DLC <sub>max</sub> @cycle no.	50th DLC	capacity retention (%)	Si:C (gram ratio)
(a) Si:SiO:C = 3:1:4	1839	933	906	1400@4	480	34	3.63:4
(b) Si:SiO:C = 2:2:4	986	523	463	1450@8	750	52	3.27:4
(c) SiO:C = 1:1	1556	693	863	870@4	610	70	2.52:4
(d) SiO:C = 1:1 (carbon coating)	1346	606	740	700@16	580	83	2.50:4

1<sup>st</sup> LC = first lithiation capacity, 1<sup>st</sup> DLC = first delithiation capacity, IRC = initial irreversible capacity, DLC<sub>max</sub> = the maximum delithiation capacity, 50<sup>th</sup> DLC = 50<sup>th</sup> delithiation capacity, capacity retention = capacity retention at 50th cycle compared to DLC<sub>max</sub>, Si:C denotes ratio of silicon and C [graphite with or without carbon coating]

Table 3. The different capacity values, capacity retention and the silicon content present in the composites.

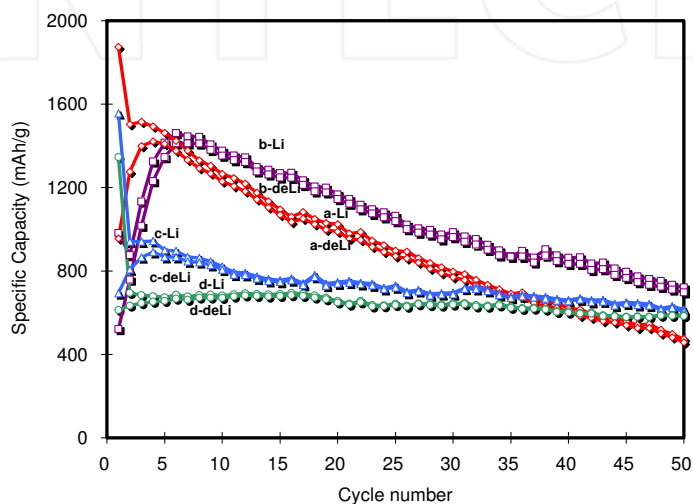


Fig. 17. Profile of capacity retention with cycling: a-Li & a-deLi, b-Li & b-deLi, c-Li & c-deLi, d-Li & d-deLi are lithiation and delithiation curves for the electrodes (a) Si:SiO:C = 3:1:4; (b) Si:SiO:C = 2:2:4; (c) SiO:C = 1:1; (d) SiO:C = 1:1 (carbon coated).

Low silicon content in the anode composite reduces the electrode strain during the lithiation and delithiation processes. The order of the capacity retention for the composite electrodes was (d) > (c) > (b) > (a). Even though the amount of carbon coating was small, its contribution to the capacity retention of the electrode was considerable; this is attributed to increase in conductivity of the electrode because of the carbon coating.

Usually delithiation capacities are lower than that for lithiation. The differences in lithiation and delithiation capacities are high when there is a high rate of decrease in capacity retention. Thus lithiation and delithiation capacities are correlated with capacity retention property.

### 5.5.2 Cyclic voltammograms of the composites (SiO/Si/C)

The lithiation and delithiation reactions that take place in the electrode may be represented in the form of equation as (9), (10) and (11).

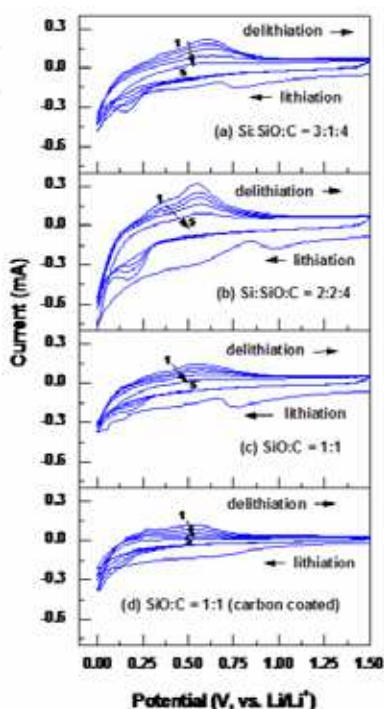
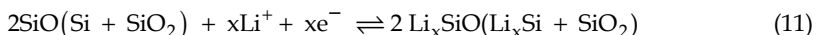
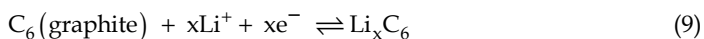
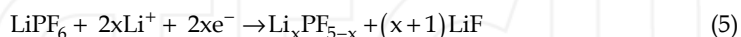


Fig. 18. Cyclic voltammograms of (a) Si:SiO:C = 3:1:4; (b) Si:SiO:C = 2:2:4; (c) SiO:C = 1:1; (d) SiO:C = 1:1 (carbon coated) with scan rate of 0.1 mV s<sup>-1</sup>.

Both forward reactions toward the formation  $Li_xC_6$  ( $x = 0$  to 1) and  $Li_xSi$  ( $x = 0$  to 4.4) or the corresponding reverse reactions (delithiation) appear to be pseudo-homogeneous phase reactions as understood from lithiation and delithiation process exhibited by the voltammograms (Fig. 18) which shows a continuous change of potential with  $x$  values. The lithiation and delithiation in graphite, silicon, and silicon monoxide are expected to occur simultaneously. The cyclic voltammogram shows higher delithiation peak currents for the composites containing silicon. The composite SiO/C devoid of silicon content and the same composite with carbon coated shows different pattern. The carbon coated one has flat peak current peak current value with potential change indicating the stability of the composite. (Schulmeister and Madar, 2003) stated that the commercial silicon monoxide is a two-phase material with regions rich in silicon and others rich in oxygen. The silicon-rich phase contains ~1000 to 2000 atoms, with the phase-separated regions having diameters of 3 - 4 nm. The silicon-rich phase alloys and de-alloys resulting in volume changes of up to ~328%.

During initial lithiation, the oxygen-rich region is converted into  $\text{Li}_2\text{O}$  following reaction (3) and remains as an inert buffer material in the subsequent cycles. Other physically bonded -O- present in the composite also forms  $\text{Li}_2\text{O}$  and serves as a volume buffer during the cycling process. Lower silicon content should provide less volume change and better capacity retention to the electrodes. Furthermore, the electrolyte undergoing decomposition into forming SEI film during the initial and subsequent cycles may be represented by the reactions (3), (5) and (12),



### 5.5.3 Comparative delithiation behaviour of composites based on Fe, Cu, Si & C

Since the delithiation properties are directly related to the amount of lithium available for lithiation process in any practical lithium ion battery, the comparative delithiation behavior of three compositions are presented in Fig. 18. The curve 'a' obtained for the composite  $\text{Fe}(1)\text{Cu}(1)\text{Si}(3.5)/\text{SPB}$  containing high silicon content does not provide good cycle life attributed to large volume expansion and crumbling of the active material. However, the same composite mixed with graphite as  $\text{Fe}(1)\text{Cu}(1)\text{Si}(3.5)/\text{Graphite}$  shown as 'b' was able to prolong the cycle life with very low capacity which is not useful. The figure clearly shows that the composition  $\text{Fe}(1)\text{Cu}(1)\text{Si}(2.5)/\text{Graphite}$  shown as 'c' depicts better capacity and high cycle life. The high performance of the  $\text{Fe}(1)\text{Cu}(1)\text{Si}(2.5)/\text{Graphite}$  is attributed to the effective buffer action of internally generated  $\text{Li}_2\text{O}$  during first lithiation process. These materials are actually double phase material as both silicon and graphite are active towards  $\text{Li}^+$  in the same potential window.

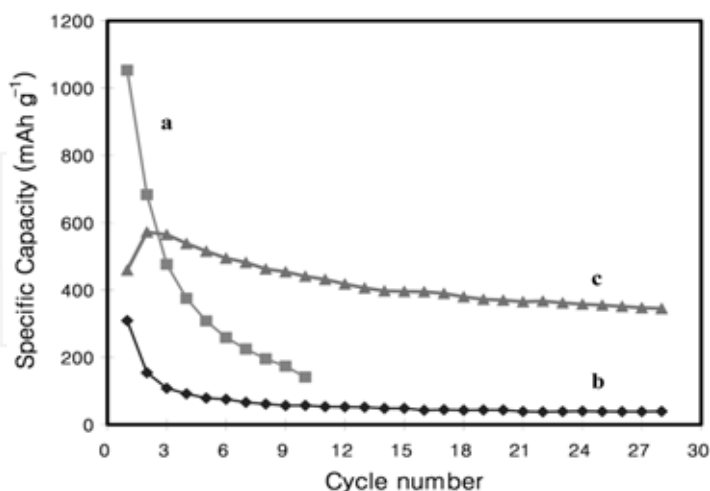


Fig. 19. Comparative delithiation behavior of a)  $\text{Fe}(1)\text{Cu}(1)\text{Si}(3.5)$  composite with Super 'T' black; b)  $\text{Fe}(1)\text{Cu}(1)\text{Si}(3.5)/\text{Graphite}$ ; c)  $\text{Fe}(1)\text{Cu}(1)\text{Si}(2.5)/\text{Graphite}$ .

## 6. Conclusion

The chapter on 'Silicon based Composite anode for Lithium ion battery' presented the state of the art on the silicon anode development and anode preparation using ball milling techniques, carbon coatings of the SiO/C anode using simple organic liquids, thermochemical treatment of the SiO with lithium hydroxide followed by ball milling with graphite and characterisation of prepared silicon anode composite through physical and electrochemical techniques.

In the composite Fe-Cu-Si/C, the metal elements act as buffer component. Both silicon and graphite participate in lithiation and de-lithiation processes. In addition the graphite has the tendency to serve as a buffer and is able to absorb volume expansion of silicon during charge/discharge process. The electrode annealed at 200 °C exhibits high initial discharge and charge capacity of 809 and 464 mAh g<sup>-1</sup>, respectively with a sustainable reversible capacity of ~385 mAh g<sup>-1</sup> at 30th cycle.

Comparative data on two different composites (1) Cu:Fe:Si = 1:1:2.5 and (2) Cu:Fe:Si = 1:1:3.5 shows that higher silicon content is deleterious to cycle performance.

The high reversible capacity ~ 690 mAh g<sup>-1</sup> at the 30th cycle by SiO/C (50:50) composite is unique in the sense that it does not involve any additional process or incorporation of a third element to act as buffers. This investigation also shows the interdependency between irreversible capacity and reversible capacity of the SiO-based system.

The charge capacity value for carbon coated carbon coated SiO/C composite anode is 500 mAh g<sup>-1</sup> where as the uncoated composite anodes shows only 318 mAh g<sup>-1</sup> at 100<sup>th</sup> cycle. The higher cycle stability in the carbon coated composite is attributed to the reinforcement of the structure by C<sub>x</sub> particles. The cyclic voltammetry study shows constant peak current value from the voltage range 0.3 to 0.6 V during delithiation which explains the compactness of the electrode structure and resistor like behaviour of the composite.

The sustained cycle capacity follow the order Si:SiO:C = 3:1:4 < Si:SiO:C = 2:2:4 < SiO:C = 1:1 < SiO:C = 1:1 (carbon coated). A comparison of the capacity and cycle stability for the composites containing silicon shows smaller silicon content favours stability of the composite electrodes.

Even though the carbon-coated composite delivered moderate capacity during cycling compared to other composites investigated, its low capacity degradation made the anode to exhibit better performance.

The heat treat treatment of (SiO + LiOH) followed by graphite mixing resulted a composition with Li<sub>4</sub>SiO<sub>4</sub>, SiO & nano-silicon particles named as (SiO + LiOH)/C gave a charge capacity ~ 333 mAh g<sup>-1</sup> at the 100th cycle with a low-capacity fade on cycling. The presence of Li<sub>4</sub>SiO<sub>4</sub> is considered to provide better charge/discharge behavior to the composite.

The discussion in the chapter shows there is ample scope replacing the graphite anode of lithium ion battery with silicon composite anode. The reason being it is environmentally benign, has higher specific capacity and prolonged cycle life. Cost effective and viable manufacturing process is possible as evident from the discussion in the chapter. Hence, the most promising anode candidate for the next generation Li-ion battery that will power automotive and other electronic gadgets will be the silicon based composite anode.

## 7. Acknowledgment

One of the authors, Angathevar Veluchamy wishes to thank Korean Federation of Science and Technology, Korea for awarding Brain Pool Fellowship for two years from October 2006

to September 2008 for the research work on anode materials for lithium ion batteries especially on 'Silicon composite anode' at Korea Electrotechnology Research Institute, Changwon, the master degree students Dong-Hun Kim and Hye-Min Shin for their support during my research period, and also the Central Electrochemical Research Institute/Council of Scientific and Industrial Research, India for granting extraordinary leave during this period.

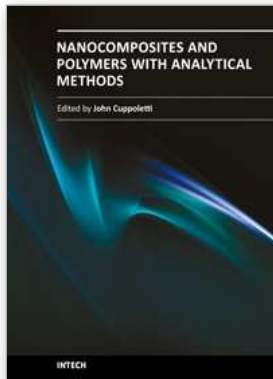
## 8. References

- Aurbach, D (2005). A review on new solutions, new measurements procedures and new materials for rechargeable Li batteries, *Journal of Power Sources*, Vol. 146, (August 2005) 71-78
- Aurbach, D. & Schechter, W. A. (2004) in: Nazri, G. A.; Pistoia, G. (Eds.). *Lithium batteries Science and Technology: Advanced Liquid Electrolyte Solution*, Kluwer Academic Publishers, Boston, (2004) 1110
- Aurbach, D. (2002) in: Schechter, W. A.; Scrosati, B (Eds.). *Advances in Lithium Ion Batteries*. Kluwer Academic, New York, (2002) 79-101
- Balasubramanian, R.; A.Veluchamy, A.; Venkatakrishnan, N & Gangadharan, R.(1995) Electrochemical characterization of magnesium silver chloride battery. *Journal of Power Sources*, 96(1995) 197-199
- Balasubramanian, R.; A.Veluchamy, A. & Venkatakrishnan, N(1994). Gasometric corrosion rate studies of magnesium alloy in magnesium batteries. *Journal of Power Sources*, Vol. 52(1994) 305-308.
- Benedek, R & Thakeray, M. M. (2002). Lithium reactions with intermetallic compound electrodes. *Journal of Power Sources*, Vol. 110(August, 2002) 406-411
- Brummer, S. B. (1980) in: Yeager, E.B.; Schumm, B.; Blomgren, G.; Blankenship, D.R.; Leger. V & Akridge. J, (Eds.). *Lithium Non-aqueous Battery Electrochemistry*. The Electrochemical Society Proceedings Series, Princeton, NJ, USA, 1980, Proc. vol. 80-7, pp. 130-142
- Cairns, E. J. & Reimer, J. A. (2002). Magnesium silicide as a negative electrode material for lithium-ion batteries. *Journal of Power Sources*, Vol. 110, (2002) 424-429.
- Chen, L, Xie, X.; Wang, B.; Wang, k & Xie, J (2006) Spherical nanostructured Si/C composite prepared by spray drying technique for lithium ion batteries anode. *Material Science and Engineering*. Vol.131(July 2006) 186-190.
- Datta, M. K. & Kumta, P. N. (2007). Silicon, graphite and resin based hard carbon nanocomposite anodes for lithium ion batteries. *Journal of Power Sources*, Vol. 165, (2007) 368-378.
- Dimove, N.; Kugino, S. & Yoshio, M. (2003). Carbon-coated silicon as anode material for lithium ion batteries: advantages and limitations. *Electrochimica Acta*, Vol. 48, (2003) 1579-1587.
- Dimove, N.; Fukuda,K.; Umeno, T.; Kugino, S & Yoshio, M. (2003). Characterization of carbon-coated silicon: Structural evolution and possible limitations. *Journal of Power sources*. Vol. 114, (February 2003) 88-95.
- Doh, C.H.; Shin, H.M.; Kim, D.H.; Jeong, Y.D.; Moon, S.I.; Jin, B.S.; Kim, H.S.; Kim, K.W.; Oh, D.H & Veluchamy, A.(2008). A new composite anode, Fe-Cu-Si/C for lithium ion battery. *Journal of alloys and compounds*, Vol. 461, (June 2008) 321-325.
- Doh, C.H.; Park, C.W.; Shin, H.M.; Kim, D.H.; Chung, Y.D.; Moon, S.I.; Jin, B.S.; Kim, H.S & Veluchamy, A.(2008). A new SiO/C anode composition for lithium -ion battery. *Journal of Power Sources*, Vol. 179 (April, 2008) 367-370.

- Doh, C.H.; Shin, H.M.; Kim, D.H.; Ha, Y.C.; Jin, B.S.; Kim, H.S.; Moon, S.I & Veluchamy, A.(2008). Improved anode performance of thermally treated SiO/C composite with an organic solution mixture. *Electrochemistry Communications* Vol. 10 (Feb, 2008) 233-237.
- Doh, C.H.; Min, H.M.; Kim, D.H.; Chung, Y.D.; Moon, S.I.; Jin, B.S.; Kim, H.S.; Kim, K.W.; Oh, D.H & Veluchamy, A.(2008). Effect of silicon content over Fe-Cu-Si/C based composite anode for lithium ion battery. *Bull. Korean Chem. Soc.*, Vol. 29 (Feb, 2008) 309-312.
- Doh, C.H.; Kim, D.H.; Lee, J.H.; Ha, K.H.; Shin, H.M.; Jin, B.S.; Kim, H.S.; Park, C.W.; Moon, S.I & Veluchamy, A.(2010). A comparative study on the performance of anodes based on SiO, Si and graphite for lithium ion battery, *Bull. Korean Chem. Soc.*, Vol. 31, No. 5, (May 2010) 1257-1261
- Doh, C. H.; Kim, D. H.; Kim, H. S.; Shin, H. M.; Jeong, Y. D.; Moon, S. I.; Jin, B. S.; Eom, S. W Kim, H. S.; Kim, K. W.; Oh, D. H.; Veluchamy, A. (January, 2008). Thermal and electrochemical behaviour of C/LixCoO<sub>2</sub> cell during safety test. *Journal of Power Sources* 175 (Jan, 2008) 881-885
- Dong, H.; Feng, R. X.; Ai, X. P.; Cao, Y. L. & Yang, H. X. (2004). Structural and electrochemical characterization of Fe-Si/C composite anode for Li-ion batteries synthesized by mechanical alloying. *Electrochimica Acta*, Vol. 49, (2004) 5217-5222.
- Dong, H.; Ai, X. P. & Yang, H. X. (2003). Carbon/Ba-Fe-Si alloy composite as high capacity anode, materials for Li-ion batteries. *Electrochemistry Communications*, Vol. 5, (2003) 952-957.
- Fleischauer, M. D.; Topple, J. M. & Dahn, J. R. (2005). Combinatorial investigations of Si-M (M = Cr + Ni, Fe, Mn) thin film negative electrode materials. *Electrochemical and solid state letters*. Vol. 8, (2005) A137.
- Fuchsbichler, B.; Stangl, C. ; Kren, H. ; Uhlig, F. & Koller, S.(March, 2011). High capacity graphite-silicon composite anode material for lithium-ion batteries. *Journal of Power Sources*, Vol. 196( March 2011) 2889-2892
- Fujifilm, Internet(1997), [http://www.fujifilm.co.jp/eng/news\\_e/nr079.html](http://www.fujifilm.co.jp/eng/news_e/nr079.html) (1996).
- Guo, Z. P.; Zhao, Z. W; Liu, H. K. & Dou, S. X. (2005). Lithium insertion in Si-TiC nanocomposite materials produced by high-energy mechanical milling. *Journal of Power Sources*, Vol. 146, (2005) 190-194.
- Huggins, R. A. & Nix & W. D. (2000). Decrepiation model for capacity loss during cycling of alloys in rechargeable electrochemical system, *Solid State Ionics*, Vol. 6, (2000) 57-63.
- Huggins, R. A. (2002). Alternative materials for negative electrodes in lithium systems. *Solid State Ionics*, Vol. 152-153, (2002) 61-68
- International Application published under the patent corporation treaty (PCT)(2004). International Publication Number WO 2004/093223 A2 dated 28.10.2004, PCT/US2004/011350.
- Jose Benedict, T.; Banumathi, S.; Veluchamy. A.; Gangadharan, R.; Zulfihar Ahemed, A. & Rajendran, S(1998). Characterization of plasticized soild polymer electrolyte by XRD and AC impedance methods. *Journal of Power Sources*, Vol. 75(1998) 171-174.
- Kim, J. B.; Jun B. S. & Lee. S. M. (2005). Improvement of capacity and cycleability of Fe/Si multilayer thin film anodes for lithium rechargeable batteries. *Electrochimica Acta*, Vol. 50, (2005) 3390-3394.
- Kim, I. S.; Kumta, P. N. & Blomgren, E. (2000). Si/TiN Nanocomposites Novel anode Materials for Li-Ion Batteries, *Electrochemical and solid state letters*. Vol. 3, (2000) 493-496

- Kim, J. H.; Kim, H. & Sohn, H. J. (2005). Addition of Cu for carbon coated Si-based composites as anode materials for lithium-ion batteries. *Electrochemistry Communications*. Vol. 7(May 2005) 557-561
- Lee, Y. S.; Lee, J. H.; Kim, Y. W.; Sun, Y. K. & Lee, S. M. (2006). Rapidly solidified Ti-Si alloy/carbon composites as anode for Li-ion batteries. *Electrochimica Acta*, Vol. 52, (2006) 1523-1526
- Lee, H. Y.; Kim, Y. L.; Hong, M. K. & Lee, S. M. (2005). Carbon-coated Ni<sub>20</sub>Si<sub>80</sub> alloy-graphite composite as an anode material for lithium-ion batteries. *Journal of Power Sources*, Vol. 141, (2005) 159-162.
- Lee, H. Y. & Lee, S. M. (2002). Graphite-FeSi alloy composites as anode materials for rechargeable lithium batteries, *Journal of Power Sources*, Vol. 112, (2002) 649-654.
- Lee, H. Y. & Lee, S. M. (2004). Carbon-coated nano-Si dispersed oxides/graphite composites as anode material for lithium ion batteries. *Electrochemistry Communications*, Vol. 6, (2004) 465-469
- Miyachi, M.; Yamamoto, H.; Kawai, H.; Ohta, T. & Shirakata, M. (2006). Analysis of SiO Anodes for Lithium-Ion Batteries. *Journal of the electrochemical society*, Vol. 152, (2005) A2089-A2091.
- Mizushima, K.; Jones, P. C.; Wiseman, P. J. & Goodenough, J. B. (1980). Li<sub>x</sub>CoO<sub>2</sub> (0<x<1): A new cathode material for batteries of high energy density. *Materials Research Bulletin*, Vol. 15, (1980) 783-789.
- Ng, S. H.; Wang, J.; Konstantinov, K.; Wexler, D.; Chew, S. Y.; Guo, Z. P. & Liu, H. (2007). Spray-pyrolyzed silicon/disordered carbon nanocomposites for lithium-ion battery anodes, *Journal of Power Sources*, Vol. 174, (2007) 823-827.
- NuLi, Y.; Wang, B.; Yang, J.; Yuan, X. & Ma, Z. (2006). Cu<sub>5</sub>Si-Si/C composites for lithium-ion battery anodes. *Journal of Power Sources*, Vol. 153, (2006) 371-374
- Panasonic's New Li-Ion Batteries Use Si Anode for 30% Higher Capacity (2010), <http://techon.nikkeibp.co.jp/article/HONSHI/20100223/180545/>
- Park, M. S.; Rajendran, S.; Kang, Y. M.; Han, K. S.; Han, Y. S. & Lee, J. Y. (2006). Si-Ni alloy-graphite composite synthesized by arc-melting and high-energy mechanical milling for use as an anode in lithium ion batteries. *Journal of Power Sources*, Vol. 158, (2006) 650-653.
- Park, M. S.; Lee, Y. J.; Rajendran, S.; Song, M. S.; Kim, H. S. & Lee, J. Y. (2005). Electrochemical properties of Si/Ni alloy-graphite composite as an anode material for Li-ion batteries. *Electrochimica Acta*, Vol. 50, (2005) 5561-5567.
- Renuka, A.; Veluchamy, A.; Venkatakrishnan, N.; Nathirabegam, S.; Chidambaram, V. R.; Sabapathi, R.(1992). Improved cycle life performance of Zn/NiOOH cells using stabilized zinc electrode. *Journal of Applied electrochemistry*, Vol.22(1992) 182-184.
- Roberts, G. A.; Cairns, E. J. & Reimer, J. A. (2002). Magnesium silicide as a negative electrode material for lithium-ion batteries, *Journal of Power Sources*, Vol. 110, (2002) 424-429
- Schulmeister, K & Mader, W. (2003). TEM investigation on the structure of amorphous silicon monoxide, *Journal of Non-Crystalline Solids* 320 (2003) 143-150
- Shi, Z.; Liu, M.; Naik, D. & Gole, J. L. (2001). Electrochemical properties of alloy electrodes for lithium batteries, *Journal of Power Sources*, Vol. 92, (2001) 70-80
- Singh, P.; Guidotti, R. A & Reisner, D. (2004). AC impedance measurements of molten salt thermal batteries, *Journal of Power Sources*, Vol. 138, (2004) 323-326.
- Veluchamy, A.; Doh, C. H.; Kim, D. H.; Lee, J. H.; Lee, D. J.; Ha, K.H.; Shin, H.M.; Jin, B.S.; Kim, H.S.; Moon, S.I & Park, C.W.(2009). Improvement of cycle behavior of SiO/C

- anode composite by thermochemically generated  $\text{Li}_4\text{SiO}_4$  inert phase for lithium battery. *Journal of Power Sources*, Vol. 188, No. 2, (Feb 2009) 574-577.
- Veluchamy, A.; Doh, C.H.; Kim, D. H.; Lee, J. H.; Shin, H. M.; Jin, B. S.; Kim, H. S. & Moon, S. I (2009). Thermal analysis of  $\text{Li}_x\text{CoO}_2$  cathode material of lithium ion battery *Journal of Power Sources*, Vol. 189(April 2009) 855-858.
- Veluchamy, A.; Ikuta, H & Wakihara, M ( 2001). Boron-substituted manganese spinel oxide cathode for lithium ion battery. *Solid state Ionics*. Vol. 143,(June, 2001)161-171
- Wang, G. X.; Sun, L.; Bradhurst, D. H.; Zhong, S.; Dou, S. X. & Liu, H. K. (2000). Innovative nanosize lithium storage alloys with silica as active centre. *Journal of Power Sources*, Vol. 88(2), (2000) 278-281
- Wang, K.; He, X.; Wang, L.; Ren, J.; Jiang, C. & Wan. C. (2007). Si, Si/Cu core in carbon shell composite as anode material in lithium ion batteries. *Solid State Ionics*, Vol. 178, (2007) 115-118.
- Weydanz, W. J.; Wohlfahrt-Mehrens, M. & Huggins, R. A. (1999). A room temperature study of the binary lithium-silicon and the ternary lithium-chromium-silicon system for use in rechargeable lithium batteries. *Journal of Power Sources*, Vol. 81-82, (1999) 237-242
- Wilson, A. m.; Zank, G.; Eguchi, K.; Xing, W. & Dahn, J. R. (1997). Pyrolysed silicon-containing polymers as high capacity anodes for lithium- ion batteries. *Journal of Power Sources*, Vol.68 (1997) 195-200.
- Wolfenstine, J. (1999). Critical grain size for micro-cracking during lithium insertion. *Journal of Power Sources*, Vol. 79, (1999) 111-113
- Wolfenstine, J. (2003)  $\text{CaSi}_2$  as an anode for lithium-ion battery, *Journal of Power Sources*, Vol. 124, (2003) 241-245.
- Yang, X.; Wen, Z.; Xu, X.; Lin, B.; Huang, S.( 2007). Nanosized silicon-based composite derived by in situ mechanochemical reduction for lithium ion batteries. *Journal of Power sources*, Vol.164,(Feb 2007) 880-884.
- Yazami, R. & Touzain, Ph. (1982). International Meeting on Lithium Batteries. Rome, April 27-29, 1982, C.L.U.P. Ed. Milan, Abstract # 23.
- Yazami, R. & Touzain, Ph. (1983). A reversible graphite-lithium negative electrode for electrochemical generators. *Journal of Power Sources*, Vol. 9, (1983) 365-371.
- Zhang, Y.; Fu, Z. W & Qin, Qi. Z.(2004). Microstructure and Li alloy formation of nano-structured amorphous Si and Si/TiN composite thin film electrodes. *Electrochemistry communications*, Vol. (May 2004) 484-491
- Zhang, X. N.; Huang, P. X.; Li, G. R.; Yan, T. Y.; Pan, G. L. & Gao, X. P. (2007). Si-AB5 composites as anode materials for lithium ion batteries, *Electrochemistry Communications*. Vol. 9, (2007) 713-717
- Zuo, P.; Yin, G. & Tong, Y. (2006). SiMn-Graphite composites as anodes for lithium ion batteries, *Solid State Ionics*, Vol. 177, (2006) 3297-3301.
- Zuo, P & Yin, G. (2006). Si-Mn composite anodes for lithium ion batteries, *Journal of alloys and compounds*, Vol. 414, (2006) 265-268.



## **Nanocomposites and Polymers with Analytical Methods**

Edited by Dr. John Cuppoletti

ISBN 978-953-307-352-1

Hard cover, 404 pages

**Publisher** InTech

**Published online** 09, August, 2011

**Published in print edition** August, 2011

This book contains 16 chapters. In the first part, there are 8 chapters describing new materials and analytic methods. These materials include chapters on gold nanoparticles and Sol-Gel metal oxides, nanocomposites with carbon nanotubes, methods of evaluation by depth sensing, and other methods. The second part contains 3 chapters featuring new materials with unique properties including optical non-linearities, new materials based on pulp fibers, and the properties of nano-filled polymers. The last part contains 5 chapters with applications of new materials for medical devices, anodes for lithium batteries, electroceramics, phase change materials and matrix active nanoparticles.

### **How to reference**

In order to correctly reference this scholarly work, feel free to copy and paste the following:

Angathevar Veluchamy and Chil-Hoon Doh (2011). Silicon Based Composite Anode for Lithium Ion Battery, Nanocomposites and Polymers with Analytical Methods, Dr. John Cuppoletti (Ed.), ISBN: 978-953-307-352-1, InTech, Available from: <http://www.intechopen.com/books/nanocomposites-and-polymers-with-analytical-methods/silicon-based-composite-anode-for-lithium-ion-battery>

# **INTECH**

open science | open minds

### **InTech Europe**

University Campus STeP Ri  
Slavka Krautzeka 83/A  
51000 Rijeka, Croatia  
Phone: +385 (51) 770 447  
Fax: +385 (51) 686 166  
[www.intechopen.com](http://www.intechopen.com)

### **InTech China**

Unit 405, Office Block, Hotel Equatorial Shanghai  
No.65, Yan An Road (West), Shanghai, 200040, China  
中国上海市延安西路65号上海国际贵都大饭店办公楼405单元  
Phone: +86-21-62489820  
Fax: +86-21-62489821